

Robust fluctuation-based super-resolution microscopy in a confocal architecture

Alexander Krupinski-Ptaszek^{1,*}, Adrian Makowski^{1,4}, Aleksandra Mielnicka²,
Monika Pawłowska¹, Ron Tenne^{3,*}, Radek Łapkiewicz¹

¹Faculty of Physics, University of Warsaw, Pasteura 5, 02-093 Warsaw, Poland

²The Nencki Institute of Experimental Biology, PAS, 02-093 Warsaw, Poland

³Department of Physics, University of Konstanz, Universitätsstraße 10, D-78457
Konstanz, Germany

⁴Laboratoire Kastler Brossel, ENS-PSL Université, CNRS, Sorbonne Université,
Collège de France, 24 rue Lhomond, Paris 75005, France

* a.krupinski-ptaszek@uw.edu.pl, ron.tenne@uni-konstanz.de

1 Abstract

Record-holding super-resolution microscopy (SRM) techniques, e.g. localization microscopy (LM) and stimulated-emission-depletion (STED) microscopy, require significant resources and effort from life-science researchers. In comparison with confocal microscopy, apart from relying on extensive sample-staining procedures and long acquisition times, applying LM for 3D and multicolor imaging poses a considerable experimental challenge. In the current work, we provide a complete demonstration of an entry-level SRM technique - providing super-resolving capabilities with an experimental complexity level akin to that of confocal microscopy. Exchanging the confocal pinhole with a small pixelated detector, we use the inherent fluctuations of dye molecules as contrast for SRM. This contrast is processed into a super-resolved image through a process of pixel reassignment, a robust and deterministic algorithm. Since the fluctuation contrast is ubiquitous to organic markers, it does not require engineering of the blinking statistics through the sample buffer. Together with the built-in capabilities for multi-color and 3D imaging, shown in our work, it can become a natural extension to confocal microscopy - a straightforward first step into the realm of SRM.

2 Introduction

Fluorescence fluctuations in molecules stand at the heart of many super-resolution microscopy (SRM) methods[1, 2, 3, 4, 5, 6]. In particular, localization microscopy (LM) that regularly achieves 20-30 nm lateral resolutions has made a significant impact on life-science imaging. However, in comparison to confocal microscopy, the tool of choice for life-science imaging, performing LM is a laborious task[7]. First, acquisition times can be prohibitively long. Second, three-dimensional (3D) and multi-color imaging remain challenging even two decades after the introduction of LM[8]. Finally, successful localization of markers requires a delicate control of the fluctuation statistics of their emission through a precise control of the sample buffer[5, 9, 10] or through controlling the dynamic binding of markers [6, 11]. These shortcomings generate a strong drive to find entry-level SRM techniques that maintain the advantages of confocal laser-scanning microscopy (CLSM), even if providing only moderate resolution enhancements. One example of these is structured-illumination microscopy[12] and its confocal variant image-scanning microscopy (ISM) [13, 14]. In ISM, replacing the confocal pinhole with a small pixelated detector improves the lateral resolution by a factor of two and increases the signal-to-noise ratio (SNR) [15, 16]. A second notable example is super-resolution optical fluctuation imaging (SOFI) in which the temporal correlation of fluctuations forms

the contrast for 3D resolution enhancement even without precise engineering of the fluctuation statistics [3, 17, 18]. Recently, we have published a proof-of-principle demonstration of a combination of SOFI and ISM, appropriately termed SOFISM[19]. Rendering the second-order correlation of the fluorescence of inorganic quantum dots (blinking) provided a x2.5 enhancement of lateral resolution beyond the diffraction limit.

The use of inorganic fluorophores, that served the majority of early SOFI demonstrations, is quite limiting due to the difficulties in incorporating them within cells and targeting specific subcellular sites[3, 17, 20]. While SOFI images have also been obtained with more common organic fluorophores, such as dye molecules[21] and fluorescent proteins[22], their inherent intensity fluctuations occur at the technologically inconvenient sub-millisecond time scale[23]. This scale is incompatible with low-light cameras such as sCMOS, which operate at best with millisecond frame-acquisition times and suffer from significant readout noise[24, 25].

In recent years, the rapid development of single-photon avalanche diode (SPAD) arrays, in which readout noise is inconsequential, enabled imaging of fluorescence dynamics with sub-nanosecond resolution, six orders of magnitude beyond standard imagers[26, 27, 28]. Utilizing the nanosecond-scale timing information, fluorescence lifetime imaging (FLIM) and quantum correlations can be measured in widefield (WF) and ISM architectures[29, 30, 31, 32, 33, 34]. In contrast, the additional capabilities of SPAD arrays at microsecond-to-millisecond time scales were only scarcely used[35, 36, 37], despite the fact that information revealed with such a camera can be instrumental for microscopy.

In the current work, we take advantage of an off-the-shelf confocal SPAD array to capture the native fluctuations of dye molecules and obtain super-resolved SOFISM images of neurological cells with a large field of view (FOV). We promote the proof-of-principle demonstration of SOFISM into a fully operational entry-level microscopy technique, performing large FOV super-resolution microscopy with standard fluorophores and without the use of a buffer. Finally, taking advantage of the pulse-to-pulse resolution of the detection, we use time multiplexing to obtain super-resolved two-color images without the need for image registration in post processing.

3 Concept

The excited state of the lowest of a dye molecule is divided into a spin-triplet and a spin-singlet state (Fig. 1a). An absorption of a photon populates the singlet ($S=0$) state and would be commonly followed by an emission of a photon and a return to the ground state. The inherent fluctuations in the emission intensity result from a transition into the triplet state - intersystem crossing. As relaxation from the triplet to the ground state is dipole forbidden, the excitation is shelved for a period of few to hundreds of microseconds, depending on the molecule and its environment. Using a standard camera, with a millisecond temporal resolution, the fluctuation dynamics is invisible and manifests only as an undesired decrease of emission yield for labels. However, when properly sampled, fluorescence dynamics are also a resource rather than a nuisance for microscopy: they provide extra information that can be applied to overcome the diffraction limit, e.g., in SOFI and LM.

In our setup (Fig. 1b), the pinhole aperture of a standard confocal microscope is replaced with a confocal 23-pixels SPAD array (SPAD23, Pi imaging). As a fluorescent sample is raster scanned across the laser focus ($\lambda=635$ nm, 40 MHz repetition rate) the detection times of emitted photons are recorded by the SPAD array (Fig. 1c, top). To form images from this dataset, we use two different pipelines: summation and correlation, described in detail in Section 1 of the supplementary information. In the first, summing the number of photons detected per scan step effectively produces a diffraction-limited confocal laser-scanning microscopy (CLSM) image (Fig. 1d, top right). Alternatively, we bin the detection time of photons with a fine resolution (10 μ s), generating an intensity time trace for each pixel and scan step (Fig. 1c, middle). Correlating these for every detector pair and performing pixel reassignment produces the super-resolved SOFISM image of the Atto643-labeled actin filaments in the sample (Fig. 1d, bottom left) [38, 19]. In pixel reassignment, a concept first introduced in the context of ISM, each pixel effectively acts as an

off-optical-axis closed pinhole in confocal scan. It, therefore, produces a $x\sqrt{2}$ -resolution-enhanced image that is slightly shifted with respect to the scan position. Combining this image-sharpening mechanism together with that provided by the correlation contrast itself (SOFI), a SOFISM image achieves an up to $x4$ enhancement of resolution beyond the diffraction limit. To highlight the effect, the two blue frames present magnified portions of the sample analyzed with CLSM and SOFISM. We note that as often done in pixel reassignment, we apply a Fourier-reweighting (FR) procedure for the SOFISM (see the Methods section and Supplementary Section 1).

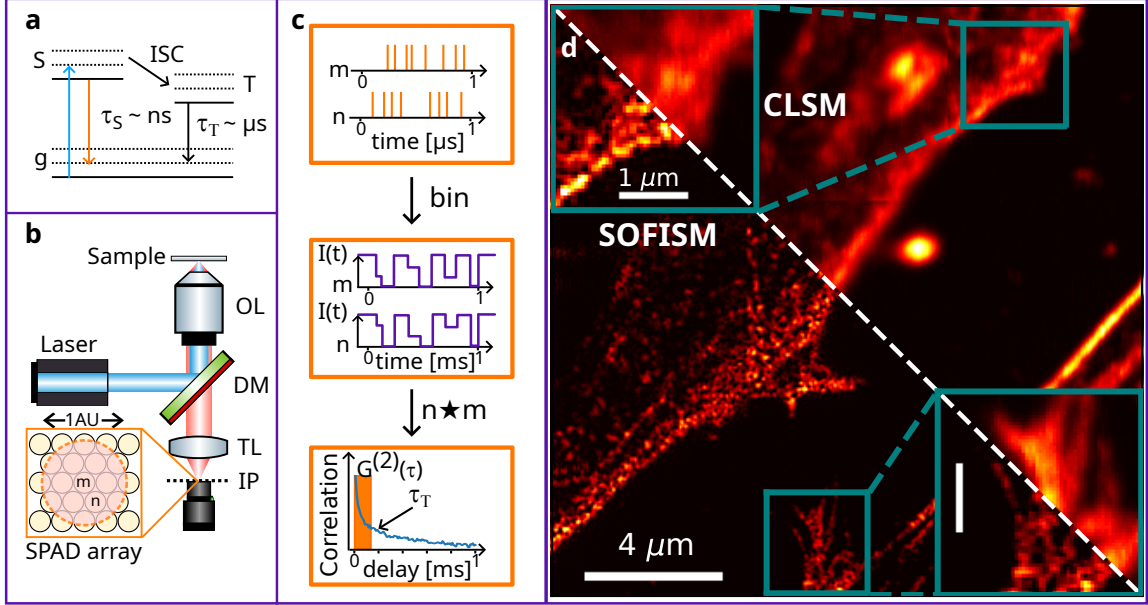


Figure 1: **The concept of SOFISM.** (a) A Jablonski diagram - the energy levels of a dye molecule. After excitation to the spin-singlet state S (blue arrow), ISC competes with radiative recombination (orange arrow) resulting in the occupation of the spin-triplet state (T). The long lifetime of the dipole forbidden transition back to the ground state (g) results in a dark period. (b) A schematic of the experimental setup. The inset shows the layout of the 23 pixels in the confocal SPAD array. (c) The SOFISM data analysis pipeline. The bottom panel present the correlation function average over the entire image shown in (d), depicting an exponential decay with time constants in the order of 100s of μs . (d) A demonstration of SOFISM imaging. A neuronal sample, in which actin filaments were stained with Atto643 dye molecules was scanned through the laser focus. The resulting image compares the CLSM analysis (top left) with SOFISM (bottom right). Blue frames present magnifications to better compare the resolution enhancement in SOFISM. To avoid color saturation, the relatively bright bottom-right portion of the image was scaled separately. The scale bar marks $4 \mu m$ in the main image and $1 \mu m$ in the magnified frames.

4 Results

For an initial demonstration of the resolution improvement in SOFISM, we performed imaging of a sparse sample of quantum dots (QDs) deposited on glass (see Methods section). The data from a scan of an exemplary scene of two quantum dots separated by approximately 200 nm was processed with CLSM, ISM, SOFISM procedures (Fig. 2a). To negate the attenuation of high spatial frequencies, we perform Fourier reweighting (FR)[13] on the SOFISM data, yielding an FR-SOFISM image (Fig. 2a). The gradual resolution improvement reflects the different contributions to the overall resolution enhancement. The QD pair is unresolved in the CLSM and ISM images, whereas SOFISM clearly separates the two emitters and FR SOFISM further refines the image. A line profile through the centers of the quantum dots is presented in the last panel of Figure 2a. For

a quantitative analysis of the resolution enhancement, we analyze 45 measurements of isolated QDs (see Supplementary Section 3). The average full width at half maxima (FWHM) of the point-spread function (PSF) in CLSM, ISM, SOFISM and FR SOFISM is 234 nm, 195 nm, 141 nm and 114 nm, respectively. For comparison, the diffraction-limited performance of the system was analyzed through wide-field imaging of the same QDs, where the average FWHM is 294 nm. Overall, FR SOFISM improves the lateral resolution by a factor of 2.58 beyond the diffraction limit. We note that with the implementation of FR, the resolution enhancement factor is somewhat dependent on the SNR of the contrast through the choice of filter parameters (see Supplementary Section 1).

Next, to verify the straightforward compatibility of SOFISM with life-science imaging, we demonstrate the method for a neuronal-cell sample over a relatively large field of view (Fig. 2). An astrocyte cell in a fixed primary-rat neuronal-cell culture, stained with phalloidin-conjugated Atto 643 dye, is imaged over a $11 \times 11 \mu\text{m}^2$ FOV. Fig. 2b and Fig. 2c present the images produced by the CLSM and SOFISM analyses pipeline, respectively. Importantly, the staining procedure used here is a common and relatively simple one where the phalloidin peptide binds to the filamentous actin (F-actin) proteins, thus visualizing the cytoskeleton of the cell. To highlight the resolution improvement, panels d and e of Fig. 2 present two representative line profiles across the white dashed lines in Fig. 2b. In contrast to the continuous CLSM contour, the correlation contrast exhibits a sharper profile with multiple distinct peaks. We note that since the labeling density in this sample was insufficient for the achieved resolution of FR SOFISM, the super-resolved images appear somewhat fragmented. Future implementations would require further optimization of the the staining procedure.

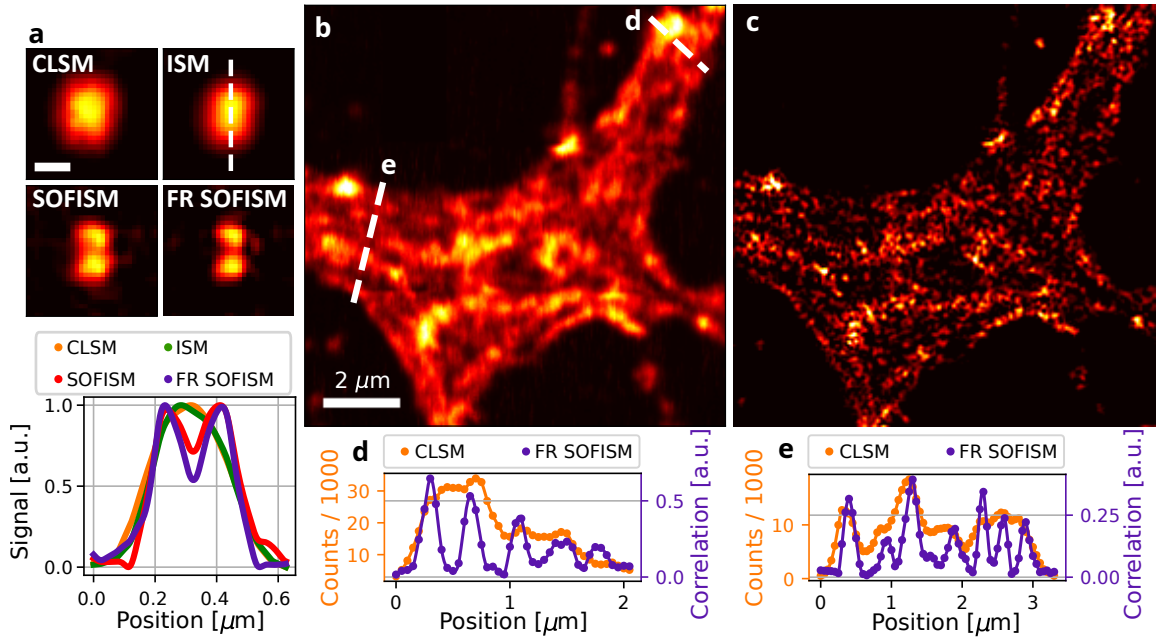


Figure 2: **Analyzing the lateral resolution enhancement of SOFISM.** (a) Comparing the resolving power of CLSM, ISM, SOFISM and FR SOFISM on a scene of two QDs separated by approximately 200 nm (top). Below, a comparison image cross sections taken along white dashed line. (b,c) A CLSM (b) and FR SOFISM (c) image contracted from the same confocal scan data for an astrocyte cell in which the cytoskeleton is marked with Atto 643 marker molecules. (d,e) Two cross sections taken along the white dashed lines in (c), highlighting the resolution enhancement of SOFISM (purple in comparison with CLSM).

The key benefit of confocal microscopy is optical sectioning - the rejection of out-of-focus contributions to the image, enabling volumetric imaging of biological specimens. Using the correlation contrast, SOFI also introduces sectioning in the axial direction. The blurred emission from a defocused plane mixes the PSFs of multiple emitters and thus reducing the level of single-point temporal

correlation. In SOFISM, both the confocal architecture and the use of the correlation contrast contribute to a 3D resolution that surpasses that of either methods separately.

To quantify the axial resolution improvement and optical sectioning capabilities of SOFISM, we scan a single QD in all three dimensions. CLSM (left) and SOFISM (right) X-Z slices are shown in Fig. 3a (Z is the direction of the optical axis). Clearly, the SOFISM contrast is localized to smaller extents in both lateral and axial directions, illustrating a 3D resolution enhancement. The white dashed line marks the location of the line profiles presented in Fig. 3b, with FWHM of 642 nm (CLSM, orange) and 389 nm (SOFISM, purple). To quantify the optical sectioning (see also Supplementary Section 4), the intensity and correlation contrast were summed across X and Y, yielding FWHM of 753 nm and 425 nm, respectively. SOFISM improves both the axial resolution of CLSM (x1.65) and the optical sectioning (x1.77) by a similar factor.

To verify the improved axial resolution of SOFISM in bioimaging, we perform 3D imaging of the sample shown in Fig. 1 within a $2 \times 2 \times 2 \mu\text{m}^3$ volume. Fig. 3c presents an X-Y image of a portion of the cell. A white box marks the region scanned in three dimensions. An X-Z CLSM slice across the white dashed line in Fig. 3c is shown in Fig. 3d. Here, the intensity is spread out across most of the scanned range. A SOFISM analysis from the same scan is shown in Figure 3e. The much narrower axial confinement of the contrast reflects the optical sectioning of SOFISM. Line profiles across the Z-axis, matching the white dashed lines in Fig. 3d, are shown in Fig. 3f. SOFISM data (purple) depicts fine features that cannot be resolved in the CLSM one (orange). In particular, the resolution improvement is clearly observed by comparing the depth of the dip at $Z=0.9 \mu\text{m}$ position in Fig. 3f between CLSM and SOFISM. All together, the results in Figs. 2 and 3 prove that SOFISM enhances the resolution in all three spatial dimensions using standard dye labels in a biological sample. All together, in FR SOFISM, the three-dimensional volume of the PSF is x7.21 (FWHM) smaller in comparison with a confocal microscope scan analyzed from the same data set.

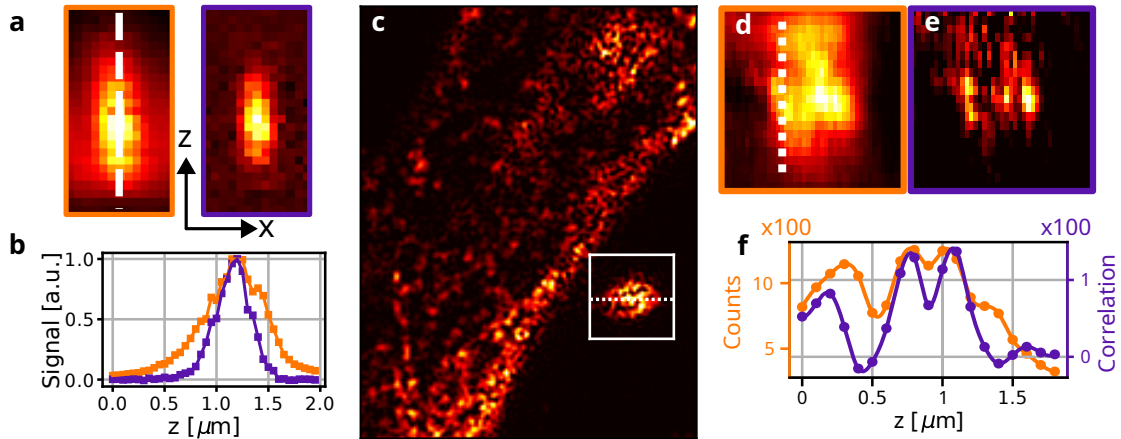


Figure 3: **Axial resolution in SOFISM.** (a) An XZ scan of an isolated QD analyzed through the CLSM (left) and SOFISM (right) pipeline demonstrating a x1.65 axial resolution improvement of SOFISM beyond a confocal microscope. (b) Cross sections along the optical axis from the CLSM (orange) and SOFISM (purple) scans in (a). (c) An FR SOFISM image of a section from the same neuronal sample shown in Fig. 1. The white frame highlights a region in which an XYZ scan was performed. An XZ section of this 3D scan (dashed line in (c)) was analyzed through the CLSM (d) and SOFISM (e) protocols. (f) A Z cross section (dashed line in (d)) demonstrating the improved axial resolution of SOFISM as compared to CLSM (orange).

Often, understanding biological structure and its relation to function relies on multi-color imaging in which two or more elements are labeled with different fluorophores. Typically, this is achieved either by sequential snapshots or by spectrally separating the emitted light. In either case, super-resolution is compromised by the need to precisely align the images from the different channels, termed image registration. In the following, we describe an implementation of two-color super-

resolved imaging by temporal multiplexing of the excitation laser pulses. The temporal resolution of the SPAD array sensor is harnessed to streamline two-color super-resolution microscopy and avoid image-registration artifacts.

In our approach, multi-color imaging is achieved by means of pulsed-interleaved excitation. Pulse trains from two lasers are synchronized with a delay of τ_C (Figure 4a). Thanks to the narrow absorption bands of dye molecules, each of the lasers exclusively excites only one type of fluorescent dye. The fluorescence excited by both lasers is then imaged through the same optical path onto a single SPAD array detector without the need to optically divide their contributions. Instead, the channels are easily separated according to the time of detection, i.e. the duration between the laser trigger and the photon detection. The histogram of measured arrival times, shown in Fig. 4b, shows two decaying exponentials with nanosecond-scale lifetimes, distinguished by their delay time from the laser trigger. Emission from AlexaFluor 488 gives rise to the first exponential (green) whereas Atto 647N emission (red) to the second. The separation of the two temporal peaks is controlled by the delay between the two excitation laser pulses (14 ns). A minimal overlap (channel cross talk) is ensured thanks to the short fluorescence lifetime of both dye molecules relative to the delay between the laser pulses.

Two-color imaging is demonstrated on a primary rat neuronal cell culture where microtubule-associated protein 2 (MAP2) is stained with AlexaFluor 488 (green) and vesicle-associated membrane protein 2 (VAMP2) is stained with Atto 647N (red). A confocal scan (ISM) of $50 \times 50 \mu\text{m}^2$ FOV of the sample is shown in Fig. 4c. MAP2 (green) is associated with the microtubules, outlining the cytoskeleton of the cell whereas the VAMP2 (red) concentrates mostly around the axons and dendrites. Subsequently, $10 \times 10 \mu\text{m}^2$ regions, marked with white dashed squares, are imaged with a finer spatial resolution and a longer scan-step dwell time (10 ms per scan step). The CLSM images of these regions are presented in Figure 4d and 4f. Vesicles (red) are typically observed in the perimeter of the main microtubule strand (green), with some signal with a defocused appearance present in the background. In comparison, Fig. 4e and 4g present the results of FR SOFISM analysis of the data presented in Fig. 4d and 4f, respectively. Co-localization of the two channels is distinctly sharpened in the SOFISM images. In addition, thanks to the improved optical sectioning, SOFISM discards the defocused background contributions of the signals in the red channel, for both images.

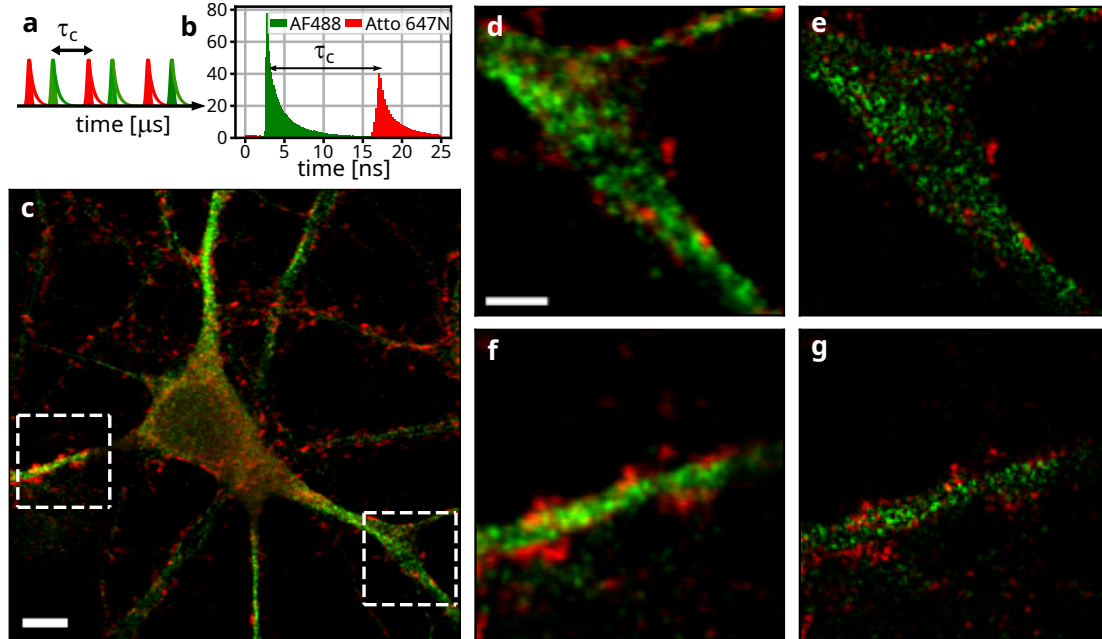


Figure 4: **Implementation of two-color super-resolution with SOFISM.** (a) Scheme of temporal multiplexing. Two laser pulse trains with an interpulse duration of 25 ns each are delayed by 14 ns with respect to each other. (b) The histogram of time delays between the trigger pulses and detection events includes two distinct peak colored with red and green corresponding to the PL of AF488 and Atto647N molecules, respectively. (c) Two ISM images from the different channels, resulting from a fast scan of a large area, are overlaid following the same color scheme of (a) and (b). The two $10\mu\text{m} \times 10\mu\text{m}$ areas marked with white dashed frames are scanned with 10 ms integration time per pixel from which CLSM (d) and (f) and FR SOFISM (e) and (g) are obtained. Scale bars: (c): $5\ \mu\text{m}$, (d): $2\ \mu\text{m}$.

5 Conclusions

In summary, we have expanded upon the recent proof-of-principle demonstration of SOFISM, proving that it provides $\times 7.2$ volumetric resolution enhancement for biological samples. The inherent microsecond-scale fluctuations in the emission of dye molecules, is captured by a small SPAD-array sensor that replaces the confocal pinhole. As such, the time-consuming engineering of fluorescence fluctuations, typical to many SRM methods, is unnecessary and the samples are buffer free. A $\times 2.09$ and $\times 1.65$ lateral and axial resolution enhancements over CLSM are demonstrated over large fields of view for an overall $\times 7.21$ decrease of the PSF volume. A straightforward extension to two color imaging is achieved by taking advantage of the ns temporal resolution of the detector.

The scale of invested experimental resources, both in terms of lab work and equipment are similar to that required for confocal imaging. In fact, since the optical setup and staining techniques are nearly identical, the transition between the two modalities is nearly seamless. Altogether, we believe that SOFISM can serve well as an entry-level SRM - achieving substantial resolution improvement in three dimensions without demanding great efforts in the preparation of the sample or in a special design of an optical setup. Given that cost-effective and low noise SPAD arrays are likely to become a part of commercial confocal microscope systems in the near future, SOFISM presents a formidable opportunity for life-science researchers as a first step into super-resolution imaging. An extension to a multifocal design, already successfully implemented for ISM[16, 39, 40], and the algorithmic merger of ISM and SOFISM together [41] will enable 3D imaging at rates close to those offered by current confocal microscopes.

6 Methods

Confocal microscopy. A custom-built microscopy setup was constructed around a Nikon Eclipse Ti2 body. Two picosecond lasers (LDH-D-C-485 and LDH-P-C-635M, PicoQuant) are overlapped on a dichroic mirror (DM) (P3-405BPM-FC-2, Thorlabs) and coupled to a polarization-maintaining single-mode fiber (P3-405BPM-FC-2, Thorlabs). The light output from the fiber is reflected from quad-edge DM (Di01-R405/488/532/635-25x36, Semrock) and focused onto the sample using an oil-immersion objective lens (CFI Plan Apo Lambda D 100X/1.45-NA, Nikon). The emitted fluorescence, transmitted through the DM, is imaged through the tube lens (TL) onto a confocal SPAD array (SPAD23, Pi Imaging) placed in the image plane (IP). Detection events providing the time and pixel number of each photons are digitally transferred to a computer for further analysis and image construction. Additional magnification is used to ensure that the SPAD array occupies approximately one Airy unit. The sample is scanned over a stationary focused excitation beam using a piezo stage (P-545.3R7 PInano with E-727.3RD Digital Multi-Channel Piezo Controller, PhysikInstrumente). Both laser and piezo stage provide input trigger pulses to the SPAD array, marking each laser pulse and scan position coordinates, respectively.

Temporal multiplexing for two-color imaging. In these experiments both laser pulses excited the sample with a time delay of 14 ns between them (see Fig. 4). The delay between the time tag of each detection and the preceding laser trigger is used to discern which of the two laser pulse trains excited this PL event. The earlier (later) peak in the histogram in Fig. 4 correspond to the 485 nm (635 nm) laser pulses which exclusively excite two dye markers. Detections delayed by -0.7 ns to 13.3 ns from the 485 nm laser pulse are considered as that of the first channel whereas the remaining events are assigned to the second channel.

Preparation of quantum-dots samples. Samples containing sparse scenes of quantum dots (QDs) for resolution assessment were prepared through drop-casting. A concentrated solution of QDs (Qdot 605 ITK, Invitrogen) was substantially diluted in toluene. A 50 μ L drop was then cast onto a microscope coverslip and left to dry in the air. To mitigate QD clustering, prior to drop casting, the QD solution underwent a 15-minute sonication bath.

References

- [1] Eric Betzig, George H Patterson, Rachid Sougrat, O Wolf Lindwasser, Scott Olenych, Juan S Bonifacino, Michael W Davidson, Jennifer Lippincott-Schwartz, and Harald F Hess. Imaging Intracellular Fluorescent Proteins at Nanometer Resolution. *Science*, 313(5793):1642–1645, September 2006.
- [2] Michael J Rust, Mark Bates, and Xiaowei Zhuang. Sub-diffraction-limit imaging by stochastic optical reconstruction microscopy (STORM). *Nature Methods*, 3(10):793–796, October 2006.
- [3] T. Dertinger, R. Colyera, G. Iyer, S. Weiss, and J. Enderlein. Fast, background-free, 3D super-resolution optical fluctuation imaging (SOFI). *Proceedings of the National Academy of Sciences of the United States of America*, 106(52):22287–22292, December 2009. Publisher: National Academy of Sciences.
- [4] Nils Gustafsson, Siân Culley, George Ashdown, Dylan M. Owen, Pedro Matos Pereira, and Ricardo Henriques. Fast live-cell conventional fluorophore nanoscopy with ImageJ through super-resolution radial fluctuations. *Nature Communications*, 7(1):12471, November 2016. Publisher: Nature Publishing Group.
- [5] Mike Heilemann, Sebastian van de Linde, Mark Schüttpelz, Robert Kasper, Britta Seefeldt, Anindita Mukherjee, Philip Tinnefeld, and Markus Sauer. Subdiffraction-Resolution Fluorescence Imaging with Conventional Fluorescent Probes. *Angewandte Chemie International Edition*, 47(33):6172–6176, August 2008. Publisher: WILEY-VCH Verlag.
- [6] Ralf Jungmann, Christian Steinhauer, Max Scheible, Anton Kuzyk, Philip Tinnefeld, and Friedrich C. Simmel. Single-molecule kinetics and super-resolution microscopy by fluorescence

- imaging of transient binding on DNA origami. *Nano Letters*, 10(11):4756–4761, November 2010. Publisher: American Chemical Society.
- [7] J. Vangindertael, R. Camacho, W. Sempels, H. Mizuno, P. Dedecker, and K. P.F. Janssen. An introduction to optical super-resolution microscopy for the adventurous biologist. *Methods and Applications in Fluorescence*, 6(2):022003, March 2018. Publisher: IOP Publishing Ltd.
- [8] Mickaël Lelek, Melina T. Gyparaki, Gerti Beliu, Florian Schueder, Juliette Griffié, Suliana Manley, Ralf Jungmann, Markus Sauer, Melike Lakadamyali, and Christophe Zimmer. Single-molecule localization microscopy. *Nature Reviews Methods Primers*, 1(1):1–27, June 2021. Number: 1 Publisher: Nature Publishing Group.
- [9] Graham T Dempsey, Joshua C Vaughan, Kok Hao Chen, Mark Bates, and Xiaowei Zhuang. Evaluation of fluorophores for optimal performance in localization-based super-resolution imaging. *Nature Methods*, 8(12):1027–1040, 2011.
- [10] Sebastian van de Linde, Anna Löschberger, Teresa Klein, Meike Heidebreder, Steve Wolter, Mike Heilemann, and Markus Sauer. Direct stochastic optical reconstruction microscopy with standard fluorescent probes. *Nature Protocols*, 6(7):991–1009, July 2011. Number: 7 Publisher: Nature Publishing Group.
- [11] Ralf Jungmann, Maier S. Avendaño, Johannes B. Woehrstein, Mingjie Dai, William M. Shih, and Peng Yin. Multiplexed 3D cellular super-resolution imaging with DNA-PAINT and Exchange-PAINT. *Nature Methods*, 11(3):313–318, March 2014. Number: 3 Publisher: Nature Publishing Group.
- [12] M. G. L. Gustafsson. Surpassing the lateral resolution limit by a factor of two using structured illumination microscopy. *Journal of Microscopy*, 198(2):82–87, May 2000. Publisher: Wiley/Blackwell (10.1111).
- [13] Claus B. Müller and Jörg Enderlein. Image Scanning Microscopy. *Physical Review Letters*, 104(19):198101, May 2010. Publisher: American Physical Society.
- [14] C. J. R. Sheppard. Superresolution In Confocal Imaging. In Henri H. Arsenault, editor, *Optik*, volume 80, pages 53–54, January 1988. Issue: 2 ISSN: 0030-4026.
- [15] Andrew G York, Sapun H Parekh, Damian Dalle Nogare, Robert S Fischer, Kelsey Temprine, Marina Mione, Ajay B Chitnis, Christian A Combs, and Hari Shroff. Resolution doubling in live, multicellular organisms via multifocal structured illumination microscopy. *Nature Methods*, 9(7):749–754, July 2012. Publisher: Nature Publishing Group.
- [16] Olaf Schulz, Christoph Pieper, Michaela Clever, Janine Pfaff, Aike Ruhlandt, Ralph H. Kehlenbach, Fred S. Wouters, Jörg Großhans, Gertrude Bunt, and Jörg Enderlein. Resolution doubling in fluorescence microscopy with confocal spinning-disk image scanning microscopy. *Proceedings of the National Academy of Sciences of the United States of America*, 110(52):21000–21005, December 2013. Publisher: National Academy of Sciences.
- [17] Peter Dedecker, Gary C. H. Mo, Thomas Dertinger, and Jin Zhang. Widely accessible method for superresolution fluorescence imaging of living systems. *Proceedings of the National Academy of Sciences*, 109(27):10909–10914, July 2012. Publisher: Proceedings of the National Academy of Sciences.
- [18] Monika Pawlowska, Ron Tenne, Bohnishikha Ghosh, Adrian Makowski, and Radek Lapkiewicz. Embracing the uncertainty: the evolution of SOFI into a diverse family of fluctuation-based super-resolution microscopy methods. *Journal of Physics: Photonics*, 4(1):012002, January 2022. Publisher: IOP Publishing.

- [19] Aleksandra Sroda, Adrian Makowski, Ron Tenne, Uri Rossman, Gur Lubin, Dan Oron, and Radek Lapkiewicz. SOFISM: Super-resolution optical fluctuation image scanning microscopy. *Optica*, 7(10):1308, October 2020. arXiv: 2002.00182 Publisher: OSA Place: Washington, D.C. ISBN: 978-1-943580-67-5.
- [20] Thomas Dertinger, Alessia Pallaoro, Gary Braun, Sonny Ly, Ted A. Laurence, and Shimon Weiss. Advances in superresolution optical fluctuation imaging (SOFI). *Quarterly Reviews of Biophysics*, 46(2):210–221, 2013. Publisher: Cambridge University Press.
- [21] Thomas Dertinger, Mike Heilemann, Robert Vogel, Markus Sauer, and Shimon Weiss. Super-resolution optical fluctuation imaging with organic dyes. *Angewandte Chemie - International Edition*, 49(49):9441–9443, December 2010. Publisher: WILEY-VCH Verlag.
- [22] Hendrik Deschout, Tomas Lukes, Azat Sharipov, Daniel Szlag, Lely Feletti, Wim Vandenberg, Peter Dedecker, Johan Hofkens, Marcel Leutenegger, Theo Lasser, and Aleksandra Radenovic. Complementarity of PALM and SOFI for super-resolution live-cell imaging of focal adhesions. *Nature Communications*, 7(1):13693, December 2016. Publisher: Nature Publishing Group.
- [23] Elana M. S. Stennett, Monika A. Ciuba, and Marcia Levitus. Photophysical processes in single molecule organic fluorescent probes. *Chemical Society Reviews*, 43(4):1057–1075, 2014. Publisher: Royal Society of Chemistry.
- [24] Osip Schwartz, Jonathan M Levitt, Ron Tenne, Stella Itzhakov, Zvicka Deutsch, and Dan Oron. Superresolution microscopy with quantum emitters. *Nano letters*, 13(12):5832–6, January 2013. Publisher: American Chemical Society.
- [25] Robin Van den Eynde, Alice Sandmeyer, Wim Vandenberg, Sam Duwé, Wolfgang Hübner, Thomas Huser, Peter Dedecker, and Marcel Müller. Quantitative comparison of camera technologies for cost-effective super-resolution optical fluctuation imaging (SOFI). *Journal of Physics: Photonics*, 1(4):044001, August 2019. Publisher: IOP Publishing Ltd.
- [26] Claudio Bruschini, Harald Homulle, Ivan Michel Antolovic, Samuel Burri, and Edoardo Charbon. Single-photon avalanche diode imagers in biophotonics: review and outlook. *Light: Science & Applications*, 8(1):87–114, December 2019. Publisher: Springer US.
- [27] Danilo Bronzi, Federica Villa, Simone Tisa, Alberto Tosi, and Franco Zappa. SPAD Figures of Merit for Photon-Counting, Photon-Timing, and Imaging Applications: A Review. *IEEE Sensors Journal*, 16(1):3–12, January 2016.
- [28] Gur Lubin, Dan Oron, Uri Rossman, Ron Tenne, and Venkata Jayasurya Yallapragada. Photon Correlations in Spectroscopy and Microscopy. *ACS Photonics*, 9(9):2891–2904, September 2022. Publisher: American Chemical Society.
- [29] Arin Can Ulku, Claudio Bruschini, Ivan Michel Antolovic, Yung Kuo, Rinat Ankri, Shimon Weiss, Xavier Michalet, and Edoardo Charbon. A 512×512 SPAD image sensor with integrated gating for widefield FLIM. *IEEE Journal of Selected Topics in Quantum Electronics*, 25(1), 2019.
- [30] Marco Castello, Giorgio Tortarolo, Mauro Buttafava, Takahiro Deguchi, Federica Villa, Sami Koho, Luca Pesce, Michele Oneto, Simone Pelicci, Luca Lanzanó, Paolo Bianchini, Colin J.R. Sheppard, Alberto Diaspro, Alberto Tosi, and Giuseppe Vicidomini. A robust and versatile platform for image scanning microscopy enabling super-resolution FLIM. *Nature Methods*, 16(2):175–178, February 2019. Publisher: Nature Publishing Group.
- [31] Jason T. Smith, Alena Rudkouskaya, Shan Gao, Juhi M. Gupta, Arin Ulku, Claudio Bruschini, Edoardo Charbon, Shimon Weiss, Margarida Barroso, Xavier Intes, and Xavier Michalet. In vitro and in vivo NIR fluorescence lifetime imaging with a time-gated SPAD camera. *Optica*, 9(5):532–544, May 2022. Publisher: Optica Publishing Group.

- [32] Gur Lubin, Ron Tenne, Ivan Michel Antolovic, Edoardo Charbon, Claudio Bruschini, and Dan Oron. Quantum correlation measurement with single photon avalanche diode arrays. *Optics Express*, 27(23):32863, November 2019. arXiv: 1910.01376 Publisher: The Optical Society.
- [33] Gur Lubin, Ron Tenne, Arin Can Ulku, Ivan Michel Antolovic, Samuel Burri, Sean Karg, Venkata Jayasurya Yallapragada, Claudio Bruschini, Edoardo Charbon, and Dan Oron. Herald Spectroscopy Reveals Exciton–Exciton Correlations in Single Colloidal Quantum Dots. *Nano Letters*, 21(16):6756–6763, August 2021. Publisher: American Chemical Society.
- [34] Bienvenu Ndagano, Hugo Defienne, Dominic Branford, Yash D. Shah, Ashley Lyons, Niclas Westerberg, Erik M. Gauger, and Daniele Faccio. Quantum microscopy based on Hong–Ou–Mandel interference. *Nature Photonics*, 16(5):384–389, May 2022. arXiv: 2108.05346 Publisher: Nature Publishing Group.
- [35] M. Kloster-Landsberg, D. Tyndall, I. Wang, R. Walker, J. Richardson, R. Henderson, and A. Delon. Note: Multi-confocal fluorescence correlation spectroscopy in living cells using a complementary metal oxide semiconductor-single photon avalanche diode array. *Review of Scientific Instruments*, 84(7):076105, July 2013.
- [36] Ivan Michel Antolovic, Samuel Burri, Claudio Bruschini, Ron A. Hoebe, and Edoardo Charbon. SPAD imagers for super resolution localization microscopy enable analysis of fast fluorophore blinking. *Scientific Reports*, 7:44108, March 2017. Publisher: Nature Publishing Group.
- [37] Eli Slenders, Marco Castello, Mauro Buttafava, Federica Villa, Alberto Tosi, Luca Lanzanò, Sami Valtteri Koho, and Giuseppe Vicidomini. Confocal-based fluorescence fluctuation spectroscopy with a SPAD array detector. *Light: Science and Applications*, 10(1):2047–7538, December 2021. Publisher: Springer Nature.
- [38] Ron Tenne, Uri Rossman, Batel Rephael, Yonatan Israel, Alexander Krupinski-Ptaszek, Radek Lapkiewicz, Yaron Silberberg, and Dan Oron. Super-resolution enhancement by quantum image scanning microscopy. *Nature Photonics*, 13(2):116–122, December 2019. Publisher: Nature Publishing Group.
- [39] Maria Ingaramo, Andrew G York, Peter Wawrzusin, Oleg Milberg, Amy Hong, Roberto Weigert, Hari Shroff, and George H Patterson. Two-photon excitation improves multifocal structured illumination microscopy in thick scattering tissue. *Proceedings of the National Academy of Sciences of the United States of America*, 111(14):5254–5259, April 2014. Publisher: National Academy of Sciences.
- [40] Shun Qin, Sebastian Isbaner, Ingo Gregor, and Jörg Enderlein. Doubling the resolution of a confocal spinning-disk microscope using image scanning microscopy. *Nature Protocols*, pages 1–18, November 2020. Publisher: Springer US.
- [41] Uri Rossman, Tali Dadosh, Yonina C. Eldar, and Dan Oron. cSPARCOM: Multi-detector reconstruction by confocal super-resolution correlation microscopy. *Optics Express*, 29(9):12772, April 2021. Publisher: Optical Society of America.

7 Acknowledgements

The authors thank D. Oron, U. Rossman, L. Beck and M. Tillmann for helpful discussions regarding the work and the paper, Wiktor Szadowiak for hardware support, and M. Stefaniuk for support with the Atto643 staining. This work was supported within “A platform for fast, label-free imaging, identification and sorting of leukemic cells” project (POIR.04.04.00-00-16ED/18-00) carried out within the TEAM-NET program of the Foundation for Polish Science, co-financed by the European Union under the European Regional Development Fund. R.T. and A.K.P. acknowledge funding by the Deutsche Forschungsgemeinschaft (DFG, German Research Foundation) Project-ID 425217212-SFB 1432. R.T. thanks the Minerva foundation for their support. Ad.M. acknowledge National

Science Centre, Poland (2023/49/N/ST7/04195) and Scholarship of French Government - Ph.D. Cotutelle/Codirection.

Contributions R.L., A.K.P. and R.T. conceived the idea for the project. A.K.P. designed the experimental setup with input from R.L., M.P., Ad.M. and R.T.. A.K.P. developed the software and performed data analysis. A.K.P. performed the optical imaging experiments with the support of M.P. and Ad.M.. The biological samples were prepared by Al.M and M.P.. R.T. and R.L. co-supervised the project. A.K.P and R.T. wrote the manuscript with contributions from all authors.

8 Supplementary information

8.1 Supplementary section 1 – Data analysis

The time-tagged data of photon detections (see Methods section) is parsed into the lines and pixels of the scan based on the stage trigger marker time. Detection in each scan pixel are then binned according to their detection time to generate microsecond-scale intensity traces (number of detected photons per 10 microsecond time bin). This results in a (23, X, Y, T) dataset, where X and Y are the image dimensions in pixels, and T is the number of ten-microsecond time-bins per scan position, typically few thousands. There are 23 X by Y pixel image series of duration T, with 50 nm spatial resolution (step size) and 10 μ s temporal resolution. A CLSM image (Fig. S1 a) is obtained by summing the data across the first and last dimension, i.e. by treating the entire array as a single detector and summing all detection during the acquisition duration. To obtain an ISM image (Fig. S1 b), the data is first summed across the fourth (time) dimension, and pixel reassignment is performed prior to summation. Note that the reassignment vectors were pre determined according to a calibration measurement of an isolated fluorescent nanobead, where the center of a 2D gaussian function is estimated for each of the 23 shifted CLSM images, resulting in 23 shift vectors s_i with respect to the central detector element. For SOFISM, the temporal correlation $G^{(2)}(\tau)$ [19] between each detector pairs is calculated for each of the (x, y) sample positions, which results in a (23, 23, X, Y, D) dataset. The first (second) dimension corresponds to the correlation values between the first (second) detector and all other detectors, the third (fourth) dimension corresponds to the first (second) dimension of the scan grid, and the last dimension D corresponds to the time-delay of the correlation function. The data is then summed across the fifth dimension in a range corresponding to delays of up to 50 microseconds, resulting in 23^2 images. Then, pixel reassignment is performed, where each of the 23^2 images is shifted by the corresponding $s_{i,j} = \frac{s_i + s_j}{2}$ vector, which is the average of ISM shift vectors s_i and s_j for SPAD array pixels i and j. The shifted images are then summed to obtain the super-resolved SOFISM image (Fig. S1 c).

In diffraction-limited imaging, the information present at high spatial frequencies is attenuated due to the decay of the Fourier transform of the point-spread function (PSF), the optical transfer function (OTF). SOFISM can be thought of as taking integer powers of the CLSM PSF, corresponding to convolutions of the CLSM OTF. Consecutive convolutions further decrease the value of the OTF at high spatial frequencies, limiting the transfer of high frequency contents through the system. To enhance the high spatial frequencies in the SOFISM images, Fourier reweighting is applied obtaining an FR SOFISM image (Fig. S1 d). Fourier reweighting is done as follows:

1. 2D Gaussian PSF of width σ is generated
2. Fourier transforms of the image and PSF (\tilde{I} and OTF , respectively) are computed
3. A filter is constructed $F = \frac{1}{OTF + \epsilon \frac{k}{k_{max}}}$, with $F(k > k_{max}) = 0$, where k are the spatial frequencies
4. The FR SOFISM image is obtained as the absolute value of the inverse Fourier transform of $F \cdot \tilde{I}$

In Figs. 1 and 2, Fourier reweighting was performed using $k_{max} = 10$, $\epsilon = 0.5$ and $\sigma = 0.21 \cdot k_{max}$, whereas in Fig. 4e and Fig. 4g $\epsilon = 2$.

Bilinear interpolation followed by spline interpolation was used to obtain the line profiles presented in the main text. Bilinear interpolation is often used to approximate values of a function of two variables on a rectilinear grid (e.g. positions in an image), and it performs linear interpolation in first dimension, followed by the same operation in the second dimension. More precisely, it calculates the number of equally-spaced pixels of the same size as the original grid and calculates their coordinates. The values are then calculated as the average of the values at 4 discrete scan grid positions, weighted by the distance of the point to these positions. The bilinear interpolation results are always presented as points (squares), and only then spline interpolation is used to obtain a line

profile, and the results are identical to the profiles obtained using ImageJ's Plot Profile tool with default settings.

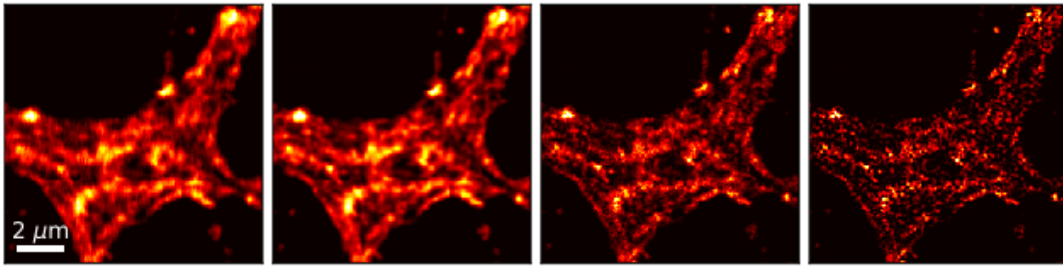


Figure 5: **Multiple image construction protocols from a single dataset.** From left to right, consecutive columns present CLSM, ISM, SOFISM and FR SOFISM images for the imaging of F-actin in an astrocyte cell presented in Fig. 2 of the main text.

8.2 Supplementary section 2 – Immunostaining

Preparation of primary-dissociated hippocampal neurons and glia co-culture for the staining procedure. All sample stainings were performed for 3-week-old primary mixed hippocampal cultures. Cells were fixed in 4% paraformaldehyde (Sigma-Aldrich®), 441244) with 4% sucrose preheated to 37°C for 10 min followed by 3 washes with PBS with 4% sucrose. After fixation, cells were permeabilized with 0.1% Triton X-100 (Bio-Rad, 1610407) in PBS for 10 min, then rinsed 3 times with PBS. Cells prepared this way were then blocked for 1,5 h in 10% goat serum (Gibco®), 16210064) in PBS to block nonspecific sites.

Immunostaining with antibodies. The cultures were incubated overnight at a temperature of 4°C in a solution containing a mixture of two primary antibodies: mouse monoclonal anti-MAP2 (Sigma-Aldrich®), M1406) diluted 1:500 in PBS with 2% goat serum and rabbit monoclonal anti-VAMP2 (D601A)(Cell Signaling Technology, 13508) diluted 1:250. After they were rinsed 3 times in PBS, the cultures were incubated 2 h at room temperature in a mixture of two various secondary antibodies: goat anti-mouse-IgG-Atto 647N (Sigma-Aldrich®), 50185) and goat anti-rabbit IgG Alexa Fluor 488 (Invitrogen, A11008) both diluted 1:500 in PBS. Cultures were mounted with Fluoromount-G (Invitrogen, 00495802).

Phalloidin staining. Subsequently, the fixed cells were stained with Atto 643-conjugated phalloidin (Atto-tec). According to the manufacturer, Atto 643 is related to Atto 647N, a popular dye for superresolution application, but has even higher photostability (Atto 643). The staining was performed according to the protocol recommended by the manufacturer (phalloidin staining). The stock solution was prepared by dissolving the 10 nmol phalloidin in methanol to yield a concentration of 10 μ M. To find the optimal emitter density, we stained the sample using 1:240 dilution of stock solution in phosphate-buffered saline (PBS) (4x more diluted than suggested by the manufacturer). Finally, the cover glasses were mounted with ProLong Glass Antifade Mountant with NucBlue nuclear stain (ThermoFisher).

8.3 Supplementary section 3 – estimating the imaging resolution

This section provides details on the determination of transverse resolution in the different imaging modalities shown within this work. For this purpose, we imaged 45 sparse scenes of quantum dots (see Methods section). These were then analyzed, using the above-mentioned protocols, to generate CLSM, ISM, SOFISM and FR SOFISM images for single isolated QDs (see examples in Fig. 6). Additionally, wide-field imaging of the same samples was performed to estimate the diffraction-limited resolution. Fitting the images to a 2D Gaussian function we determine the average FWHM of each method provided in the main text. We estimated resolution of WF, CLSM, ISM, SOFISM and FR SOFISM as 294 nm, 234 nm, 195 nm, 141 nm and 114 nm, respectively. Overall, FR SOFISM improves the lateral resolution beyond the diffraction limited wide-field imaging by a factor of 2.58, outperforming CLSM by a factor of 2.09.

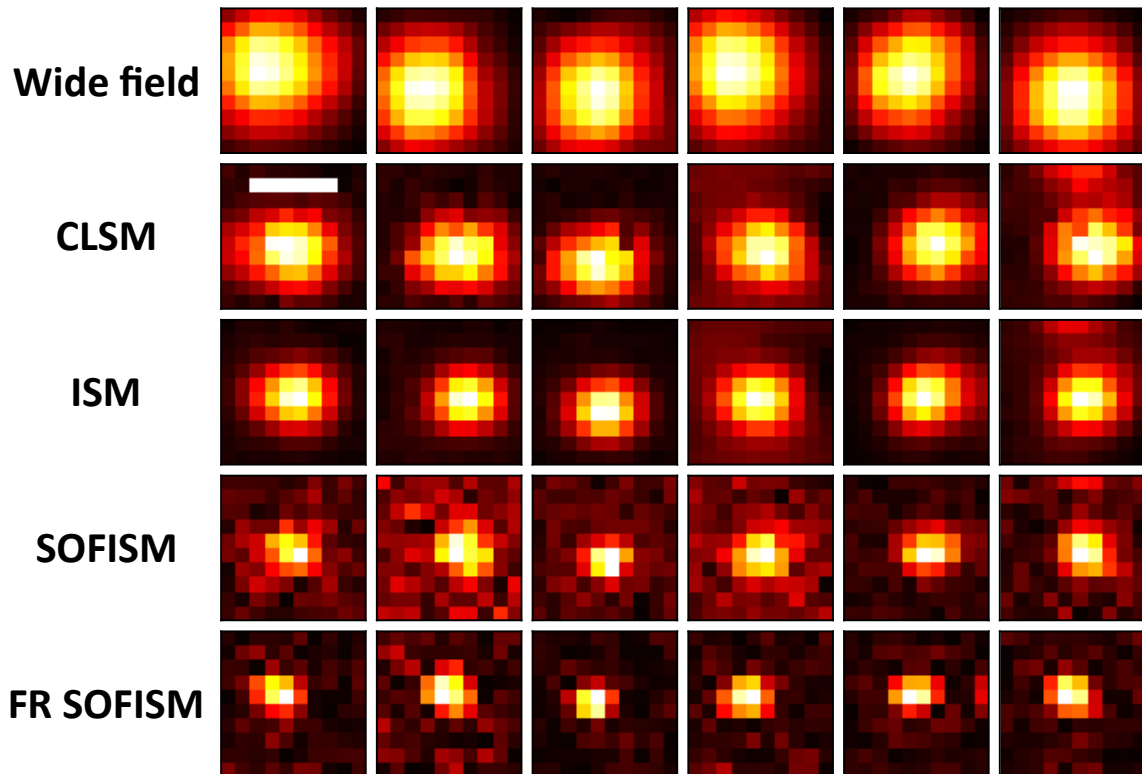


Figure 6: **QD data for transverse resolution estimate.** Each column shows a small scene around an isolated QD ($0.5\mu m \times 0.5\mu m$). From top the bottom the rows present the result of wide-field, CLSM, ISM, SOFISM and FR SOFISM analysis for the same dataset. Scale bar: 300 nm.

8.4 Supplementary section 4 – z-sectioning

Optical sectioning is one of the key features of confocal microscopy, as it enables volumetric imaging. As shown in Fig. 3 of the main text, SOFISM further improves the optical sectioning of CLSM. However, a fair comparison between the two methods requires the compensation of luminescence photo bleaching effects that deteriorate the CLSM and ISM images. The overall signal per lateral slice recorded during the acquisition of 3D data exhibits a continuous decay with a time constant of roughly 24 minutes.

The signal recorded at the beginning of the measurement sequence appears brighter than during later stages of the experiment, as shown in the maximum-intensity projections (MIPs) of raw CLSM data presented in Fig. 7a, d. The top layers exhibit high brightness decaying towards the lower regions, which correspond to later measurement times. This artifact can be mitigated by fitting the intensity values integrated over each $2\ \mu\text{m}$ by $2\ \mu\text{m}$ lateral slice of the measurement to an exponential function, as shown in Fig. 7g (red line). This data is used to estimate the overall bleaching trend as a sum of two exponential decays (black dashed line). Consequently, a correction is applied by multiplying each of the intensity slices by the inverse function of the exponential estimated value, which results in the corrected axial intensity traces shown in Fig. 3f of the main text. The position of the maximum of this corrected trace coincides with the position of the peak visible in the raw data trace, which is mostly obscured by the exponential decay. MAPs of bleaching-corrected data for the same regions shown in Fig. 7a, d are presented in Fig. 7b, e, respectively. Here, the main feature can be clearly localized slightly below the center of each image. Fig. 7c, f present MAPs of the SOFISM signal for the same scenes without any correction applied. These demonstrate a finer resolved features in the same regions. The integrated signals for each lateral slice of $1\ \mu\text{m} \times 1\ \mu\text{m}$ containing the main feature in the images are shown in Fig. S3 h, highlighting the increased optical sectioning of SOFISM (red) compared to bleaching-corrected CLSM (black). It is worth noting that since the SOFISM contrast is based on correlation of the intensity fluctuations, it is less prone to photobleaching artifacts, and requires no bleaching-correction procedures to unveil the features obscured by the prominent, out-of-focus signal present in CLSM. Lastly, Fig. 7i presents the z-sectioning analysis for the XZ scans of an isolated QD presented in Fig. 3a of the main text. As QDs are significantly more photostable than organic dyes, no bleaching correction was necessary in this case.

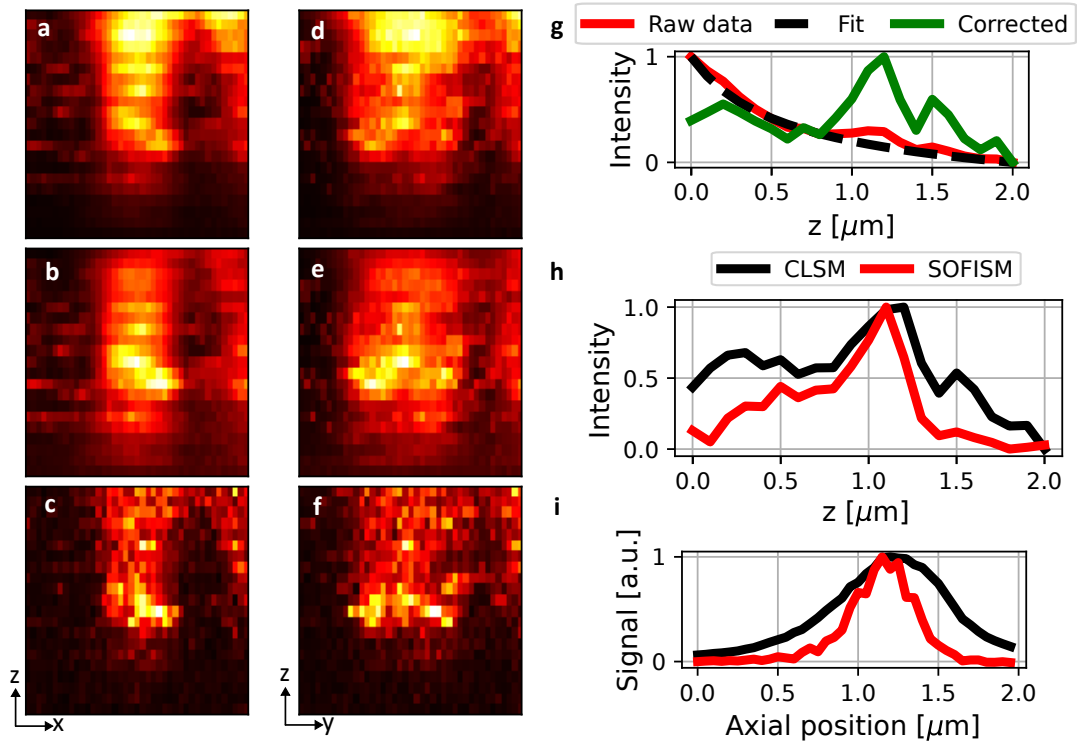


Figure 7: **Z-sectioning in SOFISM.** (a, d) Maximum intensity projections (MIPs) of the raw CLSM signal. (b, e) MIPs of the bleaching-corrected CLSM signal. (c, f) MIPs of the SOFISM signal. g) Normalized intensity recorded at each lateral plane (red), double-exponential fit (black, dashed) and the corrected intensity (green). The correction unveils the position of the main feature, obscured by the exponential decay caused by photobleaching. h) Corrected intensity (CLSM, black) and correlation (SOFISM, red) values integrated over the lateral sections containing the main feature of the dataset. The SOFISM signal exhibits a sharper peak due to superior axial sectioning. i) Sectioning analysis for the quantum dot data presented in Fig. 3 of the main text.